Investigation of Fixed Across-Track Baselines for Distributed Spaceborne SAR Systems

Francesca Scala[a], Gerhard Krieger[a], and Michelangelo Villano[a]
[a]German Aerospace Center (DLR), Microwaves and Radar Institute, Oberpfaffenhofen, Germany

Abstract

Spaceborne Synthetic Aperture Radar (SAR) greatly benefits from distributed concepts. This work investigates the opportunity of establishing formations with fixed baselines. In particular, a fixed baseline in the across-track direction can enhance the performance of SAR interferometry for the generation of accurate digital elevation models or enable multi-platform range ambiguity suppression. Achieving a fixed across-track baseline requires a continuous forced solution of the relative motion, different from the Helix configuration, adopted for TanDEM-X, which relies on a natural solution of the dynamics. Continuous control is given by low-thrust engines, which continuously compensate for the natural oscillations of the relative motion in the across-track direction and maintain the desired spacecraft separation. This study aims to evaluate the feasibility of continuous control, in terms of delta-velocity budget, and the impact on SAR interferometric performance. The analyses yield promising results in terms of SAR applications and can be used for preliminary mission analysis and design, including both SAR and mission control considerations.

1 Introduction

Across-track Synthetic Aperture Radar is a powerful technique to generate digital elevation models for accurate measurements of Earth's geophysical parameters. The power of distributed systems for across-track interferometry was demonstrated by the TanDEM-X mission, consisting of two spacecraft flying in a Helix formation [1]. TanDEM-X was able to provide accurate high-resolution Digital Elevation Models (DEMs) with single-pass SAR interferometry, avoiding the temporal decorrelation, which affects the repeat-pass approach of monolithic spacecraft architecture [1]. The high-resolution interferogram of TanDEM-X is based on the across-track baselines, realised via a Helix formation. This configuration consists of one daughter spacecraft moving on a closed trajectory, with a helical behaviour, around the mother satellite. It resulted in large baselines slowly varying in hundreds of meters range for data acquisition of the X-band SAR instrument, providing unprecedented resolution and accuracy of the digital elevation model (12 m horizontal resolution and 2 m height accuracy). Building upon these findings, this work explores a different approach for the across-track interferometry based on fixed - time invariant - baselines, when small distances (< 100 m) are involved among the platforms. Particularly, operating in the Ka-band of the electromagnetic spectrum is promising in combination with short baselines, thanks to the low penetration in the terrain [2, 3]. A similar concept of across-track fixed baselines was successfully studied for passive interferometry applications in L-band [4, 5]. To keep a constant across-track baseline among the platforms, a forced solution of the relative motion is required with continuous control. This is fundamental to avoid natural oscillations in the across-track directions and keep the desired spacecraft separation. The approach presented in this work is based on the investigation of a continuous control strategy given by low-thrust engines, such as ion or hall thrusters. Although this approach is not based on a natural solution of the relative motion, as for the Helix formation of TanDEM-X, and, consequently, it is more fuel-consuming, it provides promising results in terms of delta-v budget and DEMs performance.

This work proposes a preliminary study for the assessment of both the control effort and the performance in terms of delta-velocity budget and height accuracy, respectively, associated with different baselines. It first introduces the across-track interferometry modelling. Then, it presents the theoretical approach for the dynamical representation of a multi-satellite distributed system and the continuous control scheme. Finally, it presents the results of a parametric analysis, providing some design test cases.

2 Methodology

Maintaining constant - fixed - across-track separation among two or more platforms requires the implementation of continuous control. The corresponding generic configuration when two spacecraft are involved is shown in Figure 1. This approach presents several challenges. First, to keep a constant across-track separation, a continuous control should be implemented, resulting in a more expensive delta-velocity budget, compared to a natural solution of the relative motion. Moreover, keeping such close distances (< 100 m) requires an accurate design of control and safety procedures, to guarantee a safe flight in case of non-nominal situations (e.g., engine failures).

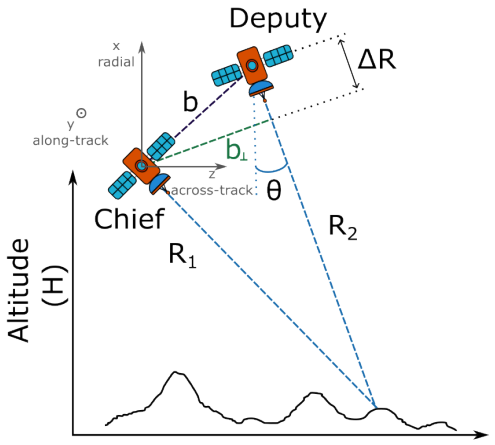

Figure 1 Two-satellites InSAR geometry.

2.1 Across-Track Interferometry

This work investigates the possibility of implementing single-pass across-track interferometry with a fixed orthogonal baseline. We selected the Ka-band for the SAR instrument to reduce penetration in the terrain and, at the same time, achieve compliant performance with a small baseline. The former aspect is important to obtain observations less affected by the penetration and accurate DEMs. Considering that the single-pass configuration avoids the temporal decorrelation, the interferogram is obtained from the combination of the images from each satellite. As shown in Figure 1, the spacecraft fly in parallel track and observe the terrain from a slightly different view angle. The baseline b corresponds to the flight path separation in the across-track direction, while the orthogonal baseline $b_\perp$ is computed from the look angle θ. During the analyses, small baselines b were assumed below 100 m. Then, depending on the coherence level γ and the number of looks n_L, the interferometric phase error $\sigma_{\psi_{\text{INT}}}$ was computed from numerical correlation [3]. Finally, the height accuracy σ_h and, specifically, the 90^{th} percentile was evaluated, as it represents an important preliminary indicator of DEMs performance.

2.2 Formation Concept

As described in Section 2.1, we propose a distributed system of multiple platforms, with one Chief or Mother spacecraft and N Deputies or Daughter satellites. The absolute orbit of the Chief can be described by the Keplerian elements $\mathbf{el}_c = \{a,\, e,\, i,\, \Omega,\, \omega,\, M\}$, where a is the semi-major axis, e is the eccentricity, i is the inclination, Ω is the right ascension of the ascending node, ω is the argument of perigee, and M is the mean anomaly. Similarly, the Keplerian elements for the j-th Deputy, with $j = 1, 2, ..., N$, are expressed as $\mathbf{el}_j = \{a,\, e,\, i,\, \Omega,\, \omega,\, M\}_j$. The motion of the Deputies around the Chief satellite can be conveniently represented with Relative Orbital Elements (ROEs) [6]. For the j-th Deputy, the ROEs can be expressed as:

$$\boldsymbol{\delta\alpha} = \begin{Bmatrix} \delta a/a \\ \delta\lambda \\ \delta e_x \\ \delta e_y \\ \delta i_x \\ \delta i_y \end{Bmatrix} = \begin{Bmatrix} (a_j - a_c)/a \\ u_j - u + (\Omega_j - \Omega)\cos i \\ e_j \cos\omega_j - e\cos\omega \\ e_j \sin\omega_j - e\sin\omega \\ i_j - i \\ (\Omega_j - \Omega_c)\sin i \end{Bmatrix}. \quad (1)$$

A first-order linear mapping is introduced to map the ROEs into the classical relative Cartesian coordinates $\{x, y, z\}$. The x coordinate represents the radial direction connecting the centre of the Earth and the Chief satellite; the z coordinate is in the normal or across-track direction, corresponding to the angular momentum direction of the Chief's orbit; and, finally, the y coordinate completes the right-hand side coordinate system, in the along-track direction (see Figure 1). The first-order linear mapping of ROEs into relative Cartesian states is given by the following expression [6]:

$$\begin{cases} x/a = & \delta a/a - \delta e_x \cos u - \delta e_y \sin u \\ y/a = & -\frac{3}{2}(u - u_0)\delta a/a + \delta\lambda + 2\delta e_x \sin u \\ & -2\delta e_y \cos u \\ z/a = & \delta i_x \sin u - \delta i_y \cos u \\ v_x/v = & \delta e_x \sin u - \delta e_y \cos u \\ v_y/v = & -\frac{3}{2}\delta a/a + 2\delta e_x \cos u + 2\delta e_y \sin u \\ v_z/v = & \delta i_x \cos u + \delta i_y \sin u \end{cases}, \quad (2)$$

where $u = nt$, with n the mean motion of the the Mother satellite: $n = \sqrt{\mu/a^3}$, and t the time variable; and $\mu = 398600\,\text{km}^3/\text{s}^2$ is the Earth gravitational parameter.

2.2.1 Relative Dynamics

The relative dynamic for close proximity operations is typically represented by the classical Hill-Clohessy-Wiltshire (HCW) equations [6]. The HCW were derived assuming pure Keplerian motion of the spacecraft involved, a quasi-circular orbit of the Mother spacecraft, and linear dynamics. In this work, we retain those assumptions, but the representation of the relative dynamics is based on the ROEs representation to better include the orbital perturbations. Specifically, we included the effect of the mean Earth's oblateness J_2 and the differential atmospheric drag. Thanks to the linear assumptions, it is possible to represent the equations of motions in terms of the State Transition Matrix (STM) for the ROEs state vector. Considering $\boldsymbol{\delta\alpha} = \{\delta a/a,\, \delta\lambda,\, \delta e_x,\, \delta e_y,\, \delta i_x,\, \delta i_y\}$, the equations of motion can be expressed as [7]:

$$\boldsymbol{\delta\alpha}(t) = \left(\boldsymbol{\Phi}_{hcw}(t) + \boldsymbol{\Phi}_{j2+drag}(t)\right)\boldsymbol{\delta\alpha}(0), \quad (3)$$

where $\boldsymbol{\Phi}_{hcw}(t)$ includes the unperturbed contribution, while $\Phi_{j2+drag}(t)$ includes the Earth's oblateness and the differential drag effects. The effect of the Keplerian relative motion is represented by:

$$\boldsymbol{\Phi}_{hcw}(t) = \begin{bmatrix} 1 & 0 & 0 & 0 & 0 & 0 \\ -1.5n & 1 & 0 & 0 & 0 & 0 \\ 0 & 0 & 1 & 0 & 0 & 0 \\ 0 & 0 & 0 & 1 & 0 & 0 \\ 0 & 0 & 0 & & 1 & 0 \\ 0 & 0 & 0 & 0 & 0 & 1 \end{bmatrix}. \quad (4)$$

The inclusion of J_2 and the differential drag requires the introduction of an augmented state $\boldsymbol{\delta\alpha}^*$, to include the drifts in the semi-major axis $\delta\ddot{a}$ and in the relative eccentricity components $\delta\ddot{e}_x$ and $\delta\ddot{e}_y$. The corresponding STM has the following expression:

$$\boldsymbol{\Phi}_{j2+drag}(t) = \begin{bmatrix} \boldsymbol{\Phi}_{j2} & \boldsymbol{\Phi}_{drag} \\ \mathbf{0}_{3\times6} & \mathbf{I}_{3\times3} \end{bmatrix}. \tag{5}$$

The full derivation and expressions of the $\boldsymbol{\Phi}_{j2+drag}(t)$ state transition matrix can be found in [7].

2.2.2 Guidance and Control Strategy

This section defines the strategy for the formation control to keep the spacecraft across-track separation rigid. To maintain the configuration in Figure 2, a continuous control procedure should be implemented on-board to compensate for both the natural oscillation of the across-track components and the external perturbations. The control aims to keep the across-track separation fixed, and equal to the initial conditions:

$$\mathbf{x}_0 = \{x,\, y,\, z,\, v_x,\, v_y,\, v_z\}_0 = \{0,\, 0,\, z_0,\, 0,\, 0,\, 0\}\,, \tag{6}$$

where the quantity z_0 corresponds to the across-track separation shown in Figure 2. The corresponding guidance in the ROEs framework is expressed as:

$$\delta\alpha_{gui}(t) = \begin{cases} \delta a/a(t) = 0 \\ \delta\lambda(t) = 0 \\ \delta e_x(t) = 0 \\ \delta e_y(t) = 0 \\ \delta i_x(t) = z_0/a\sin u \\ \delta i_y(t) = -z_0/a\cos u \end{cases}. \tag{7}$$

Once the guidance has been defined, the control strategy is derived. Continuous control is envisioned to keep the desired across-track separation, which can be obtained with low-thrust engines, such as ion or hall thrusters. The effect of the control is described in the Cartesian frame as acceleration components $\boldsymbol{a} = \{a_x,\, a_y,\, a_z\}$. To properly include the control effort in the ROEs state space representation of the dynamics, a proper control matrix $\mathbf{B}$ is introduced. Starting from the time-derivative of the dynamics, the control term is included in the state space representation:

$$\boldsymbol{\delta\dot{\alpha}} = \mathbf{A}\boldsymbol{\delta\alpha} + \mathbf{B}\boldsymbol{a}, \tag{8}$$

where $\mathbf{A}$ is the plant matrix of the system, and the matrix $\mathbf{B}$ is defined as [8]:

$$\mathbf{B} = \frac{1}{n\,a}\begin{bmatrix} 0 & 2 & 0 \\ -2 & 0 & 0 \\ \sin u & 2\cos u & 0 \\ -\cos u & 2\sin u & 0 \\ 0 & 0 & \cos u \\ 0 & 0 & \sin u \end{bmatrix}. \tag{9}$$

The corresponding forced state space response in terms of the STM is the following:

$$\begin{aligned} \delta\alpha(t) &= \boldsymbol{\Phi}\delta\alpha(t_0) + \int_{t_0}^{t} e^{\mathbf{A}(t-\tau)}\mathbf{B}(\tau)\boldsymbol{a}(\tau)\mathrm{d}\tau \\ &= \boldsymbol{\Phi}\delta\alpha(t_0) + \mathbf{B}^*\boldsymbol{a} \end{aligned}, \tag{10}$$

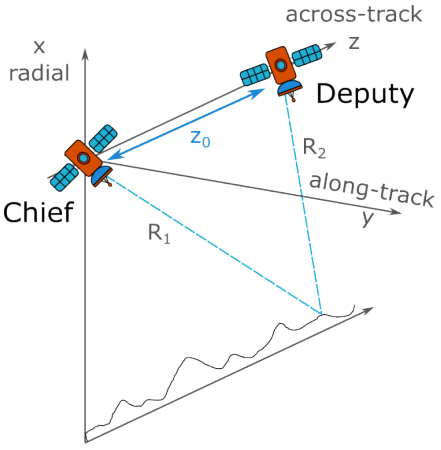

Figure 2 Across-Track Interferometric SAR geometry in the radial, along-track, and across-track reference frame ($\{x, y, z\}$).

where $\boldsymbol{\Phi}$ is the STM of the system, and $\mathbf{B}^*$ is the control matrix obtained considering that the control vector $\boldsymbol{a}$ is piece-wise constant in the manoeuvre interval $dt = t - t_0$. The full expression for matrix $\mathbf{B}^*$ is:

$$\mathbf{B}^* = \frac{1}{n^2\,a}\begin{bmatrix} 0 & 2\,ndt & 0 \\ -2\,ndt & -3/2(ndt)^2 & 0 \\ -\Delta cu & 2\Delta su & 0 \\ -\Delta su & -2\Delta cu & 0 \\ 0 & 0 & \Delta su \\ 0 & 0 & -\Delta cu \end{bmatrix}, \tag{11}$$

where Δcu and Δsu stands for $(\cos u - \cos u_0)$ and $(\sin u - \sin u_0)$, respectively.

3 Results

This section is divided into two parts. First, an analytical insight is provided in terms of continuous control effort to maintain a certain across-track separation. It delineates a procedure for the estimation of the control acceleration and the delta-velocity budget to keep the across-track separation between the satellites. Second, a parametric analysis is presented to assess both the control effort and the preliminary interferometry performance, in terms of height accuracy. The test case scenario under analysis in this work considers a constant and fixed across track separation z_0; a null radial and along track separation; a null relative velocity. The formation of two or more spacecraft is set up in the Low Earth Orbit environment, including the mean J_2 and differential drag effect.

3.1 Safety considerations

It is important to address safety considerations within the formation. Specifically, the relative motion is designed under a fully forced motion counteracting natural dynamics. This approach results in a continuous thrusting action, leading to a higher propellant consumption. In addition, in the event of an engine failure, immediate evasive manoeuvres become essential to mitigate potential collision

risk among the platforms. This approach requires a high level of autonomy of the space platform, from both the navigation and the control aspects. While safety analyses for similar configurations have been undertaken, as in [9], the criticality of this aspect to mission safety imposes the need for dedicated analyses and design. This should include on-board absolute and relative navigation systems and autonomous evasive manoeuvres, ensuring a prompt transition to safe mode for off-nominal behaviour.

3.2 Scenario definition

In this study, we consider a formation of two satellites performing across-track SAR interferometry in the Ka-band. Table 1 presents the orbital parameters and the SAR parameters considered in the analyses. An important value is the area-to-mass ratio A/m of the two spacecraft. Specifically, it influences the ballistic coefficient, which is defined as $BC = C_D \frac{m}{C_d A}$ and represents the ability of the body to overcome the atmospheric drag resistance. The drag coefficient C_D is generally selected between 2.0 and 3.0 for satellites and depends on various factors, such as the shape of the body, the solar panels' orientations, etc. [10]. Regarding the relative motion, when the A/m of two spacecraft is the same, no differential effect is generated by the drag perturbation; while it becomes significant when the two values differ. Consequently, we perform two analyses: a) equal area-to-mass ratios $(A/m)_D = (A/m)_C$, b) the area-to-mass ratio of the deputy is half the one of the chief $(A/m)_D = 0.5(A/m)_C$. Finally, concerning SAR parameters, we assume a look angle equal to 35 deg, and a number of looks equal to 24. The look angle is essential to compute the orthogonal baseline $b_\perp$ from the spacecraft separation z_0.

3.3 Analytical approach for the unperturbed case

Starting from the state space representation in Eq. 10, an analytical expression is derived for the evaluation of the control effort to keep certain guidance for the unperturbed case. For the HCW approximation, we consider the state transition matrix in Eq. 4 in the dynamical representation of Eq. 10. Imposing the guidance conditions of Eq. 7, first,

Orbital Parameters	**Value**
Altitude Range [km]	[200; 1000]
Baseline range [m]	[5; 100]
Chief's orbit type	Sun-Synchronous, quasi-circular
Earth Oblateness J_2	$1082.63 \cdot 10^{-6}$
Atmospheric model	U.S. Standard Atmosphere 1976
Chief's $(A/m)_C$ [m^2/kg]	0.0109, 0.0109
Deputy's $(A/m)_D$ [m^2/kg]	0.0109, 0.0095
SAR Parameters	**Value**
Look angle [deg]	35
Frequency [GHz]	35.5
Bandwidth [MHz]	100 MHz
No. of Looks	24

Table 1 Orbital and SAR parameters for the across-track interferometry analyses.

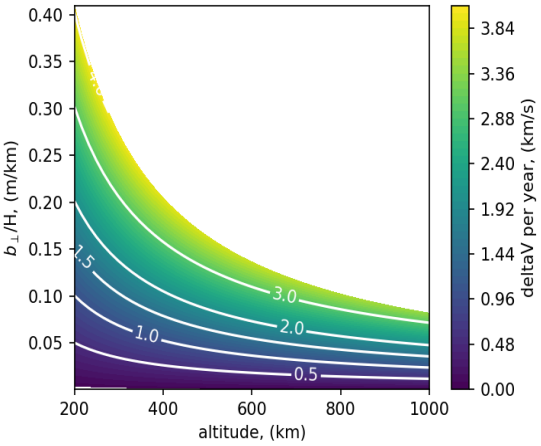

Figure 3 Yearly delta-v budget for unperturbed HCW relative motion.

we obtain the trivial solution for the acceleration components in radial and along-track directions: $a_x = a_y = 0$. Then, the out-of-plane relative motion can be solved for the a_z control acceleration component.

$$\begin{cases} \delta i_x(t) = \delta i_x(t_0) + \frac{1}{n^2}\left(\sin(nt) - \sin(nt_0)\right) a_z \\ \delta i_y(t) = \delta i_y(t_0) - \frac{1}{n^2}\left(\cos(nt) - \cos(nt_0)\right) a_z \end{cases} . \tag{12}$$

Substituting the relations in Eq. 7, and considering the initial time $t_0 = 0$, we obtain the control component in the normal direction to keep the initial conditions (i.e. pure across-track separation) as $a_z = n^2 z_0$. This component only depends on the initial separation z_0 and on the Chief's orbit mean motion n. Consequently, continuous constant control is required to keep the initial across-track separation. For mission design purposes, this control effort should be translated into a delta-velocity budget Δv. This quantity only depends on the control acceleration and on the control time Δt:

$$\Delta v = a_z \Delta t = n^2 z_0 \Delta t. \tag{13}$$

This expression is an important relation for the preliminary estimation of the control effort for an across-track formation, depending on the separation and orbital parameters of the Chief satellite. Figure 3 shows the map for the delta-velocity budget over one year. The x-axis reports the orbit altitude H, while the y-axis the ratio between the orthogonal baseline $b_\perp$ and the orbit altitude H. The orthogonal baseline $b_\perp$ is computed from z_0 and the antenna look angle (35 deg). We consider the orbit altitude of the Chief's satellite varying between 200 km and 1000 km, and z_0 varying between 5 m to 100 m, as in Table 1. Figure 3 demonstrates that the altitude has a minimal influence on the delta-v budget, while the orthogonal baseline drives the results. The primary impact of the altitude on the delta-v is a slight reduction in the control effort as the altitude increases for a fixed baseline. The delta velocity varies from a minimum of about 400 m/s per year for an initial separation of 10 m, increasing to more than 3 km/s per year when considering large baseline-to-altitude ratios.

3.4 Parametric analysis for the perturbed case

The preliminary delta-v budget of Section 3.3 serves as an initial step for a more comprehensive analysis that includes external perturbations, such as Earth's oblateness and differential drag. It evaluates the performance of the across-track interferometry for each $b_\perp/H$ configuration. The initial conditions in Table 1 are considered and the results are provided for two situations: a) $(A/m)_D = (A/m)_C$, b) $(A/m)_D = 0.5(A/m)_C$. The objectives of this section are: assessing the delta-v budget for formation maintenance and, concurrently, evaluating the height accuracy σ_h for SAR performance. Additionally, we have considered the continuous thrust required to maintain the absolute orbit under the atmospheric drag perturbation:

$$a_{drag} = -0.5\,\rho\,C_D\frac{A}{m}v^2, \tag{14}$$

where ρ is the atmospheric drag and v is the spacecraft velocity. In a preliminary approximation, the delta-v to keep the orbit altitude is computed as the integral of a_{drag} over time. The analysis implements a closed-loop control strategy for maintaining the across-track separation during SAR acquisition. The closed-loop control strategy uses a Linear Quadratic Regulator (LQR) [9] to feedback on the control accelerations on the relative dynamics. This approach not only offers an initial estimation of the delta-velocity budget but also assesses the control accuracy of the relative distance between the spacecraft. The results are shown in the form of parametric maps, for the orbit altitude H and the ratio between the orthogonal baseline $b_\perp$ and orbit altitude H. Figure 4 shows the results of the analyses for the two cases: a) $(A/m)_D = (A/m)_C$ on top, and b) $(A/m)_D = 0.5(A/m)_C$ on bottom. Both graphs exhibit similar delta-v budgets, with a slight difference for altitudes below 400 km. Specifically, case (b) results in a higher control cost for orbit maintenance due to a larger area-to-mass ratio. When comparing these results with the analytical solution in Figure 3, we can observe how the inclusion of the external perturbations, coupled with the drag compensation on the absolute orbit altitude, contributes to a more expensive control cost, particularly at lower altitudes. The analytical approach provides a reliable approximation of the control cost for formations at altitudes higher than 600 km, while it fails to accurately represent the delta-v level for altitudes below 400 km. At such lower altitudes, both the absolute and differential drag effects significantly influence the spacecraft's equation of motion, resulting in a delta-v up to 10 times higher than in the unperturbed case. A final consideration comes from comparing the results in Figure 4 with payload performance. Specifically, considering the parameters in Table 1, we compute the SAR height accuracy $\sigma_{h,p90}$ (90^{th} percentile) for various orthogonal baseline to altitude ratios, and different coherence levels. Figure 5 presents these results, where coherence levels vary within the range $[0.5, 0.99]$. The figure shows how the height accuracy improves with larger $b_\perp/H$ ratios and higher coherence levels. Furthermore, Figure 5 can be used in combination with Figure 4 for preliminary mission design. For instance, considering a $b_\perp/H = 0.05$, we can

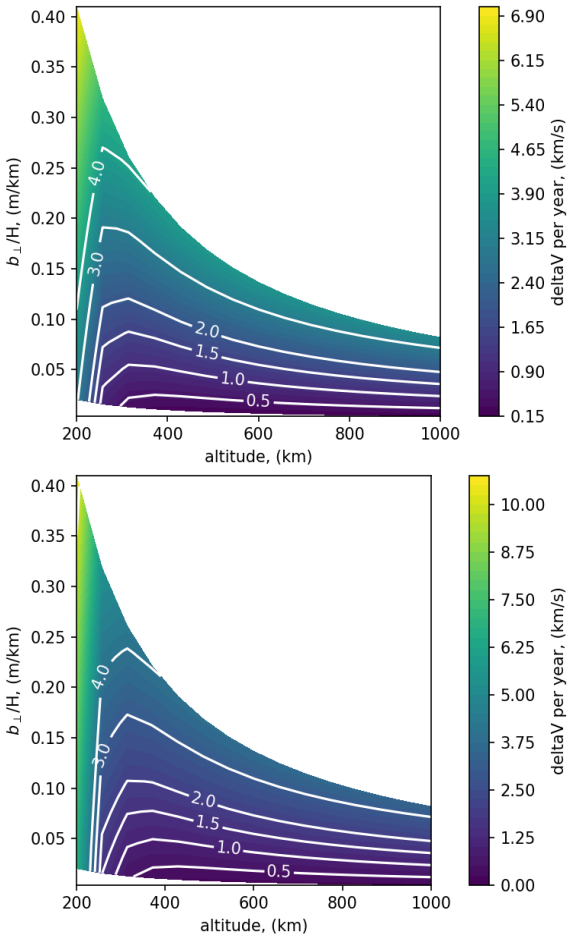

Figure 4 Yearly delta-v budget for the formation and altitude maintenance: on the top case (a), with $(A/m)_D = 0.0095$, on the bottom case (b), with $(A/m)_D = 0.0109$.

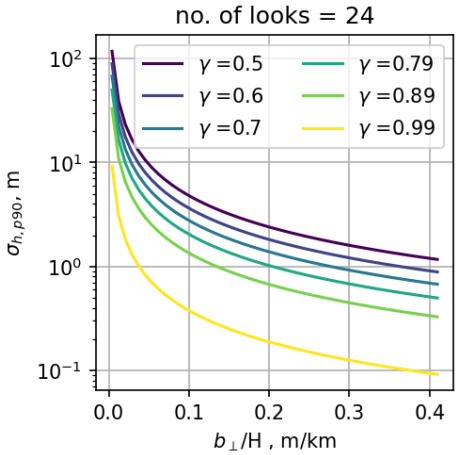

Figure 5 Hight accuracy $\sigma_{h,p90}$ (90^{th} percentile) for various $b_\perp/H$ ratios coherence levels.

identify the best high accuracy of 1 m for a $\gamma = 0.99$ and 24 looks, from Figure 5. At the same time, the same ratio in Figure 4 identifies the minimum delta-v budget of approximately 1 km/s per year at an altitude of about 500 km. This approach can be iteratively applied for each $b_\perp/H$ ratio, facilitating a trade-off between orbit altitude and SAR performance. Depending on the SAR parameters, this analysis

provides a preliminary assessment of the delta-v requirements for both formation and absolute orbit maintenance in fixed across-track baseline geometries.

3.5 Final Considerations

The previous section delineates the outcomes of the parametric analysis for the identification of the delta-v budget required by the formation and orbit maintenance. It demonstrates the synergy of the parametric maps with DEMs performance indicators (see Figure 5) for preliminary mission design. Nonetheless, the feasible levels of delta-v in Figure 4 require further consideration. Depending on the chosen baseline and altitude parameters, different levels of delta-v are identified, ranging from a few hundred to several thousand meters per second annually. This has a crucial role in the mission design procedure, influencing not only platform specifications but also mission longevity and onboard operations. Specifically, Earth observation missions in LEO typically operate with an annual delta-v budget well below the 1.5 km/s threshold, which can be seen as an upper limit during initial mission design. Conversely, larger delta-v requirements may be accommodated by incorporating such formation configurations as short operational phases, to mitigate the impact on the overall budget.

4 Conclusions

This study proposes a feasibility analysis for fixed across-track baseline interferometry. The presented analyses yield promising outcomes concerning control effort and interferometric performance. Specifically, this work marks the initial phase in delineating various mission scenarios, including the delta-velocity budget, altitude, and spacecraft separation considerations. Large across-track separations or orbit altitudes below 400 km demand high delta-v levels, making it a plausible option for a space mission with a more concise lifespan (e.g., a few years). Similarly, such configurations can be considered as short phases during the mission lifetime. Conversely, conditions requiring lower delta-v (e.g., below 1.5 km/s per year) could represent a new reference for across-track interferometry missions. In summary, these analyses constitute a preliminary investigation aimed at identifying diverse mission scenarios capable of targeting varying high accuracy levels from an interferometric perspective.

Funding Sources

This work was partially funded by the European Union (ERC, DRITUCS, 101076275). Views and opinions expressed are however those of the authors only and do not necessarily reflect those of the European Union or the European Research Council Executive Agency. Neither the European Union nor the granting authority can be held responsible for them.

5 Literature

[1] G. Krieger, A. Moreira, H. Fiedler, I. Hajnsek, M. Werner, M. Younis, and M. Zink, "TanDEM-X: A satellite formation for high-resolution SAR interferometry," IEEE Transactions on Geoscience and Remote Sensing, vol. 45, no. 11, pp. 3317-3341, Nov. 2007, doi: 10.1109/TGRS.2007.900693.

[2] S. Huber, M. Younis, and G. Krieger, "The TanDEM-X mission: overview and interferometric performance," International Journal of Microwave and Wireless Technologies, vol. 2, no. 3-4, pp. 379–389, 2010. doi: 10.1017/S1759078710000437.

[3] A. Moreira, P. Prats-Iraola, M. Younis, G. Krieger, I. Hajnsek and K. P. Papathanassiou, "A tutorial on synthetic aperture radar," in IEEE Geoscience and Remote Sensing Magazine, vol. 1, no. 1, pp. 6-43, March 2013, doi: 10.1109/MGRS.2013.2248301.

[4] M. Martín-Neira, M. Piera, F. Scala, C. Colombo, A. Zurita and B. Duesmann, "Formation Flying L-Band Aperture Synthesis Mission Concept," IEEE International Geoscience and Remote Sensing Symposium 2022, Kuala Lumpur, Malaysia, 17-22 July 2022.

[5] F. Scala, C. Colombo, B. Duesmann, M. Martin-Neira. "Analysis and design of future multiple satellite formation flying L-band missions in low Earth orbit," Proceedings of the International Astronautical Congress 2022, Paris, France, 18-22 September, 2022.

[6] S. D'Amico. "Relative orbital elements as integration constants of Hill's equations." German Aerospace Center (DLR), Technical Note TN: 05-08, 2005.

[7] A. W. Koenig, T. Giuffanti, S. D'Amico. "New State Transition Matrices for Spacecraft Relative Motion in Perturbed Orbits," Journal of Guidance, Control, and Dynamics,40:7, 1749-1768, 2017, doi: 10.2514/1.G002409.

[8] G. Gaias, M. Lovera. "Trajectory Design for Proximity Operations: The Relative Orbital Elements' Perspective," Journal of Guidance, Control, and Dynamics, 44:12, 2294-2302, 2021, doi: 10.2514/1.G006175.

[9] F. Scala, C. Colombo and M. Martìn-Neira. "A decentralised approach for formation flying reconfiguration and maintenance using GNSS-based navigation," AIAA 2022-2463. AIAA SCITECH 2022 Forum. January 2022.

[10] P. M. Mehta, A. Walker, E. Lawrence, R. Linares, D. Higdon, J. Koller. "Modeling satellite drag coefficients with response surfaces," Advances in Space Research, Volume 54, Issue 8, 2014, Pages 1590-1607, doi:10.1016/j.asr.2014.06.033.